Supporting information to **Adsorption of amphiphilic grafted polymers as polymer corrosion inhibitors: insights from mesoscopic simulations**

Javier Diaz [1], Marko Soltau[2], Martin Lísal[3,4], Paola Carbone[5], and Ignacio Pagonabarraga[1,6,7]

[1] CECAM, Centre Européen de Calcul Atomique et Moléculaire, École Polytechnique Fédérale de Lausanne, Batochime - Avenue Forel 2, Lausanne, 1015 Switzerland
[2] Straetmans High TAC GmbH, Hamburg, Germany
[3] Department of Molecular and Mesoscopic Modelling, The Czech Academy of Sciences, Institute of Chemical Process Fundamentals, Prague, Czech Republic
[4] Department of Physics, Faculty of Science, Jan Evangelista Purkyně University in Ústí nad Labem, Czech Republic
[5] Department of Chemical Engineering, The University of Manchester, Oxford Road, M13 9PL, Manchester, United Kingdom
[6] Departament de Física de la Matèria Condensada, Universitat de Barcelona, Martí i Franquès 1, Barcelona, 08028 Spain
[7] Universitat de Barcelona Institute of Complex Systems (UBICS), Universitat de Barcelona, Barcelona, 08028 Spain

March 31, 2022

1 Dissipative particle dynamics: full model description

In this section we provide a complete description of the model and complements the brief overview of the main text. The DPD model is a particle-based approach in which the material that composes the system is modelled as a collection of point particles that represents lumps of the material. Each DPD particle possess a position $\mathbf{r}_i$, mass m_i and velocity $\mathbf{v}_i$. The dynamics of the particle position is controlled by the Newton equation with the force acting on the ith particle $\mathbf{f}_i = \sum_j \mathbf{f}_{ij}$,

$$\frac{d\mathbf{r}_i}{dt} = \mathbf{v}_i \tag{S1}$$

and

$$m_i \frac{d\mathbf{v}_i}{dt} = \mathbf{f}_i \tag{S2}$$

.

In DPD all forces are pairwise additive and separable into three contributions

$$\mathbf{f}_{ij} = \mathbf{f}_{ij}^C + \mathbf{f}_{ij}^R + \mathbf{f}_{ij}^D \tag{S3}$$

corresponding to the conservative, random and dissipative forces, respectively. The conservative force is derived from a potential $\mathbf{f}^C = -\nabla V(r_{ij})$ that depends on the interparticle distance between center of masses $r_{ij} = |\mathbf{r}_i - \mathbf{r}_j|$. The potential $V(r_{ij})$ is a corse-grained potential that specifies the interaction between beads.

The dissipative and random forces also act in the direction of the interparticle separation vector $\mathbf{r}_{ij} = \mathbf{r}_i - \mathbf{r}_j$, and effectively account form the coarse-grained degrees of freedom,

$$\mathbf{f}_{ij}^D = -\gamma_{ij}\omega^D(r_{ij})\,(\hat{\mathbf{r}}_{ij}\cdot\mathbf{v}_{ij})\,\hat{\mathbf{r}}_{ij} \tag{S4}$$

for the dissipative force and

$$\mathbf{f}_{ij}^R = \sigma_{ij}\omega^R(r_{ij})\frac{\xi_{ij}}{\sqrt{\Delta t}}\hat{\mathbf{r}}_{ij} \tag{S5}$$

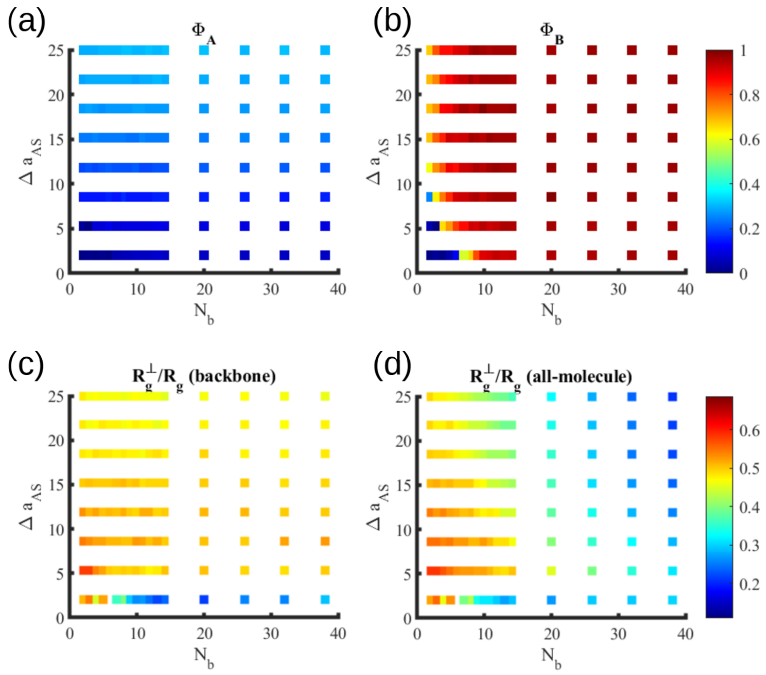

Figure S1: **Colormaps corresponding to the phase diagram N_b vs Δa_{AS} in figure 4** in the main text. 4 observables are presented: Fractions of A and B beads absorbed at the walls Φ_A and Φ_B in (a) and (b), respectively. Additionally the perpendicular to overall radius of gyration of the backbone and the full molecule, in (c) and (d), respectively. (a) and (b) share the same colorbar scale, as well as (c) with (d).

for the random force contributions. The unit interparticle vector is $\hat{\mathbf{r}}_{ij} = \mathbf{r}_{ij}/r_{ij}$ and the relative velocity is $\mathbf{v}_{ij} = \mathbf{v}_i - \mathbf{v}_j$. The weight functions $\omega^D(r)$ and $\omega^R(r)$ vanish for $r > r_c$ with r_c being the cut-off radius for DPD interactions. Parameter γ_{ij} is the friction coefficient and σ_{ij} is the noise amplitude. The Gaussian noise ξ_{ij} has zero mean and unit variance and is independent for each pair of interacting particles, while Δt is the time step. In order to satisfy the fluctuation-dissipation theorem, the weight functions are related by

$$\omega^D(r) = \left[\omega^R(r)\right]^2 \tag{S6}$$

and

$$\sigma_{ij}^2 = 2\gamma_{ij} k_B T \tag{S7}$$

where the standard form for the weight functions are

$$\omega^D(r) = \left[\omega^R(r)\right]^2 = \left(1 - \frac{r}{r_c}\right)^2 \tag{S8}$$

for $r < r_c$ and zero otherwise. Similarly, following Groot and Warren[Groot and Warren(1997)], the conservative unbonded force is often chosen as

$$\mathbf{f}_{ij}^{C,u}(r_{ij}) = a_{ij}\left(1 - r_{ij}/r_c\right)\hat{\mathbf{r}}_{ij} \tag{S9}$$

for $r < r_c$ and zero otherwise. The prefactor a_{ij} is the maximum repulsion between two particles i and j and again r_c specifies the cut-off of the DPD interaction. Additionally, particles belonging to a molecule experience bonded interaction corresponding to the connection between beads in the polymer chain. We select a harmonic spring potential of the type

$$f_{i,i+1}^{C,b} = -K\left(r_{i,i+1} - r_0\right)\hat{\mathbf{r}}_{i,i+1} \tag{S10}$$

acting between two consecutive beads i and $i+1$. The parameter K is the spring constant and r_0 is the equilibrium distance.

2 Colormaps of observables for the phase diagram of N_b vs Δa_{AS}

The phase diagram in figure 4 in the main text is constructed based on the values of the observables characterising the sorption and conformation behaviour at the surface. To facilitate reproducibility, figure S1 shows the colourmaps of the different observables.

3 Sorption diagram for molecule with weakly adsorbing side chains

In figure 4 of the main text we have explored the adsorption and conformation of strongly interacting side chain B beads with the walls. Contrary to that, in figure S2 we perform the same parameter space exploration for weakly interacting side chains, $\Delta a_{BW} = -7.5$, assigned based on the calibration curve in figure 2 (a). A less rich phase diagram can be observed in figure S2 (a) and (b), respectively for LGD ($m = 60$) and HGD ($m = 20$) molecules. As a consequence of the less favourable B-wall interaction, we only observe two types of behaviour: (1) all-molecule adsorption, driven by the overall poor solvent that leads to the segregation of the molecule into the surface; and (2) free molecule in which the solvent is not bad enough for the molecule to adsorb at the wall.

4 Role of backbone length

In the collapsed morphology in figure 4 in the main text (ie, the blue squares phase points), the backbone acquired a collapsed, isotropic shape in the vicinity of the walls. This is a consequence of the insolubility of the backbone beads leading to a micellar morphology. Nonetheless, given the heterogeneity of the molecule, we study the role of the backbone length, in order to assert whether non-isotropic conformations of the backbone may occur. 4 In figure S3 the backbone length is explored under two assumption: *I.* maintaining the spacing between grafted chains fixed $m = 60$, we assure that the ratio of A and B beads in the system remains constant. *II.* keeping the number of side chains fixed, which leads to a larger ratio of A over B beads in the molecule. In both cases the logarithmic plot shows a uniform scaling of the radius of gyration of the A beads in the system. This suggests that there is no conformational transition in the collapsed backbone, which simply grows in size as the number of A beads is increased.

A simple scaling hypothesis can assume that the collapsed A-rich globule is an isotropic sphere with radius $R_0 = \sqrt{3/5}R_g$. If we assume a uniform density of A beads $\rho_A \sim \rho$ within the isotropic globule, we express

$$R_g = \frac{\sqrt{3/5}}{\left(\frac{4}{3}\pi\rho\right)^{1/3}} N_A^{1/3} \tag{S11}$$

which is shown to approximately capture the scaling in figure S3. Deviations from this simple scaling hypothesis are more pronounced for shorter backbone lengths, where the backbone shape can be expected to be less isotropic, as the molecule conformation is more dependent on the side chain acting as anchors.

5 Formation of droplet in bulk

In the second part of the main text we explore finite concentrations of amphiphillic grafted molecules. The solubility of the backbone in amphiphillic grafted polymers has been shown to lead to rich phase behaviour[Borisov and Zhulina(20
Here we explore the role of the lyophibicity of the backbone beads in the micelle formation in the bulk (ie, in the absence of walls). Periodic boundary conditions are therefore introduced along all dimensions of the system.

In figure S4 we explore the cluster formation for a moderate number density $\rho_{mol}/\rho = 0.1$, where ρ_{mol} is the number density of beads belonging to molecules, for a molecule with configuration $300 - 38 - 60$ and the same standard interaction parameters as described in table 1 . In (a) the lyophobicity of the backbone is explored via Δa_{AS}. An approximate value $\Delta a_{AS} \sim 3$ can be identified as critical, below which we observe a uniform distribution of molecule beads. This can be mapped into a critical Flory-Huggins parameter $\chi_{AB}^{crit} \sim 0.86$, which signals the transition from the Θ solution into the formation of micelles. In (b), in such regime the cluster size distribution indicates an algebraic decay (open symbols). Contrary to that, strongly lyophobic backbone beads lead to the formation of micelles and a well-defined cluster size in (b).

In (c), (d) and (e) we show the radial distribution function of bead pairs with species backbone-branches (AB), branches-solvent (BS) and backbone-solvent (AS), respectively. The transition from the Θ solution of backbone to the micelle formation is clear in (e), where solvent beads are expelled from the micelles, while the backbone solubility clearly plays no role in the branches-solvent pair distribution in (d), due to the branches neutral interaction with the solvent.

6 Additional figures corresponding to the monodisperse nondilute case (fig. 5)

In order to support the curves shown in figure 5 we include figure S5 where we show the density curves (left column) and snapshots (right column) for three representative number densities: $\sigma_B^* = 0.6$ (a) and (b), $\sigma_B^* = 3.6$ (c) and (d) and $\sigma_B^* = 7.9$ (e) and (f). The curves in the left show the vertical densities for a distance y away from the adsorbing walls, for the two molecule species: backbone (A,in red) and side chains (B, in blue). The

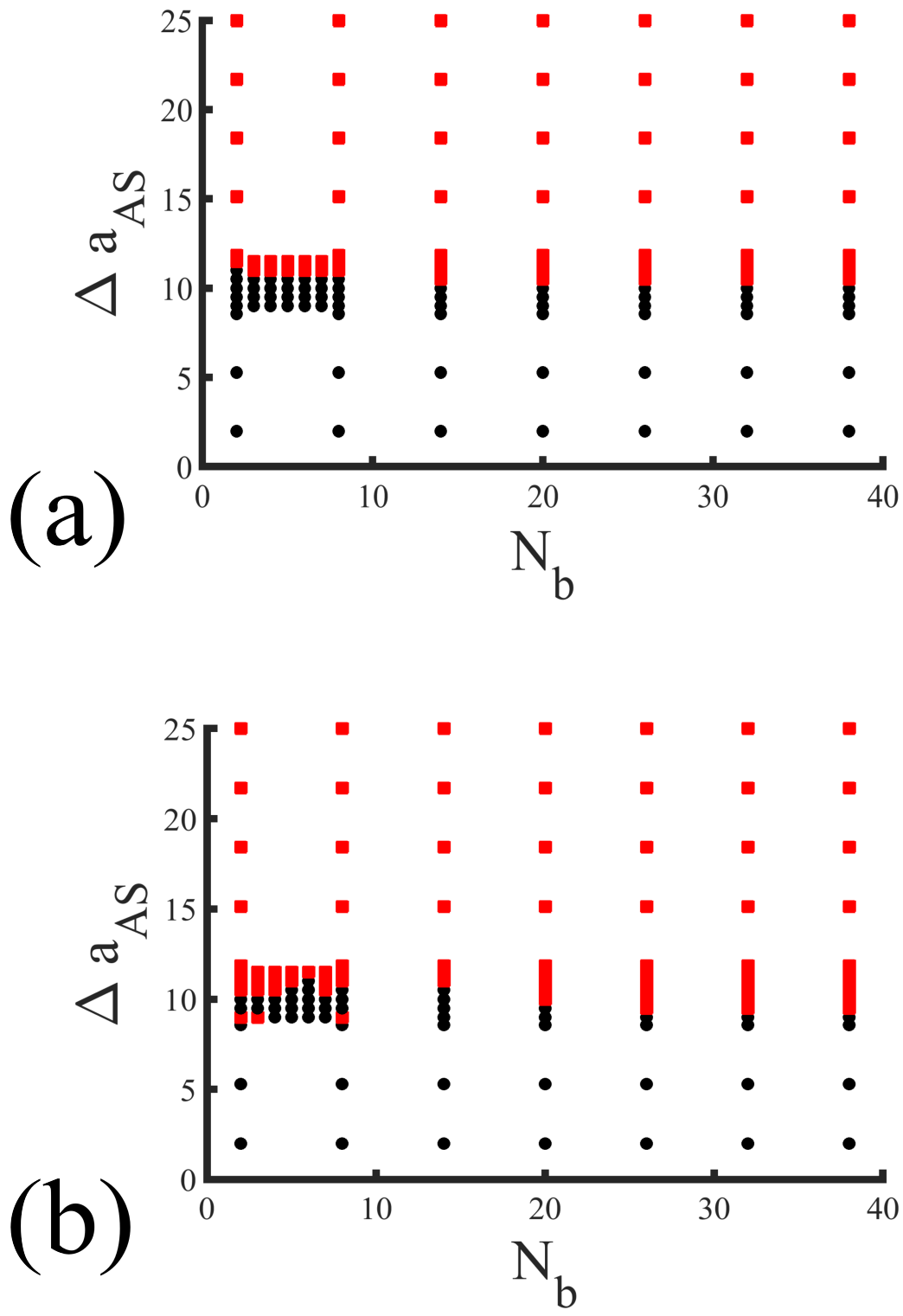

Figure S2: **Sorption diagram of a molecule** with weak branch-wall interaction $\Delta a_{BW} = -7.5$. The molecule is $300 - N_b - m$ with backbone solubility given by Δa_{AS}. Two grafting densities are explored in (a) LGD and (b) HGD, respectively $m = 60$ and $m = 20$. The phase point schematic representation are shown in the right, corresponding to: black dot, non-adsorbed; and red asterisk, all-molecule weakly adsorbed. Phase points are determined *via* observables described in section 2.3 .

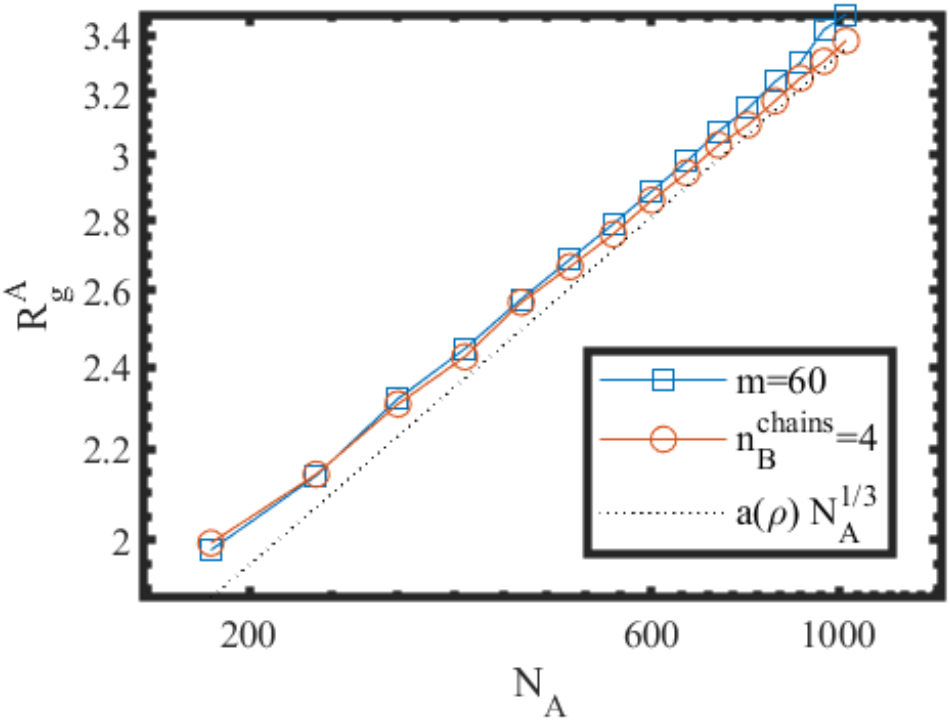

Figure S3: **Role of backbone length** N_A in the A bead radius of gyration R_g^A. Two limiting cases are considered: fixed $m = 60$ spacing between grafted side chains, and fixed number of side chains $n_B^{chains} = 4$. For comparison, the scaling $a(\rho)N_A^{1/3}$ with $a(\rho) = \sqrt{3/5}/(4/3\pi\rho)^{1/3}$.

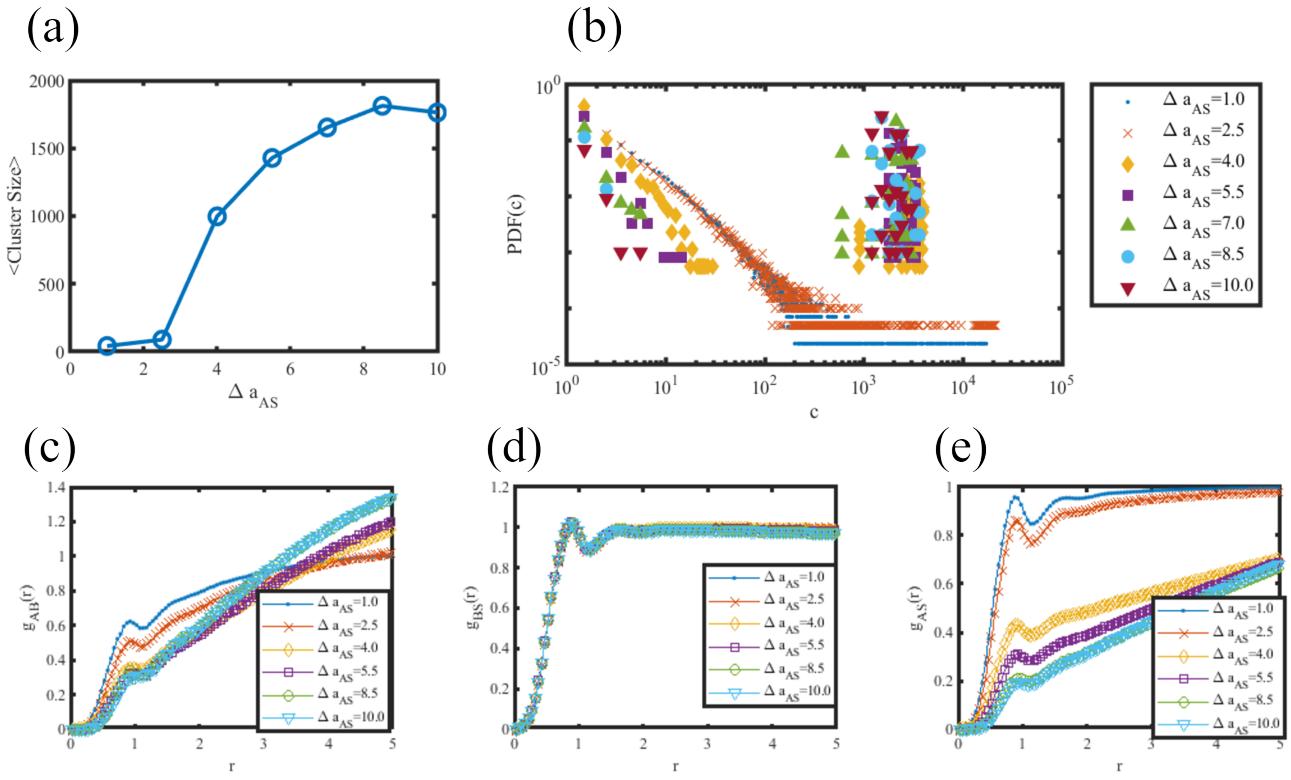

Figure S4: Cluster formation of amphiphillic molecule $300 - 38 - 60$ in bulk for different solvent quality by increasing the lyophobicity of the backbone *via* Δa_{AS} . The molecule bead concentration is $\rho_m/\rho = 0.1$. In (a) the mean cluster size in terms of the backbone insolubility and in (b) the cluster size distribution in log-log scale. A high frequency of zero values of the PDF $PDF(c) = 0$ is due to the discrete nature of the micelle, when formed, which are constituent of a discrete number of molecules with each molecule made of a large number of beads. In (c), (d) and (e) we show the radial distribution function $g_{ij}(r)$ of beads pairs of species backbone-branches (AB), branches-solvent (BS) and backbone-solvent (AS), respectively.

emergence of secondary density peaks of side chains away from the surface is clear in (c) and (e). In the right column $X - Z$ plane is shown, in order to facilitate the visualisation of the the system.

References

[Groot and Warren(1997)] R. D. Groot and P. B. Warren, *The Journal of Chemical Physics*, 1997, **107**, 4423–4435.

[Borisov and Zhulina(2005)] O. V. Borisov and E. B. Zhulina, *Macromolecules*, 2005, **38**, 2506–2514.

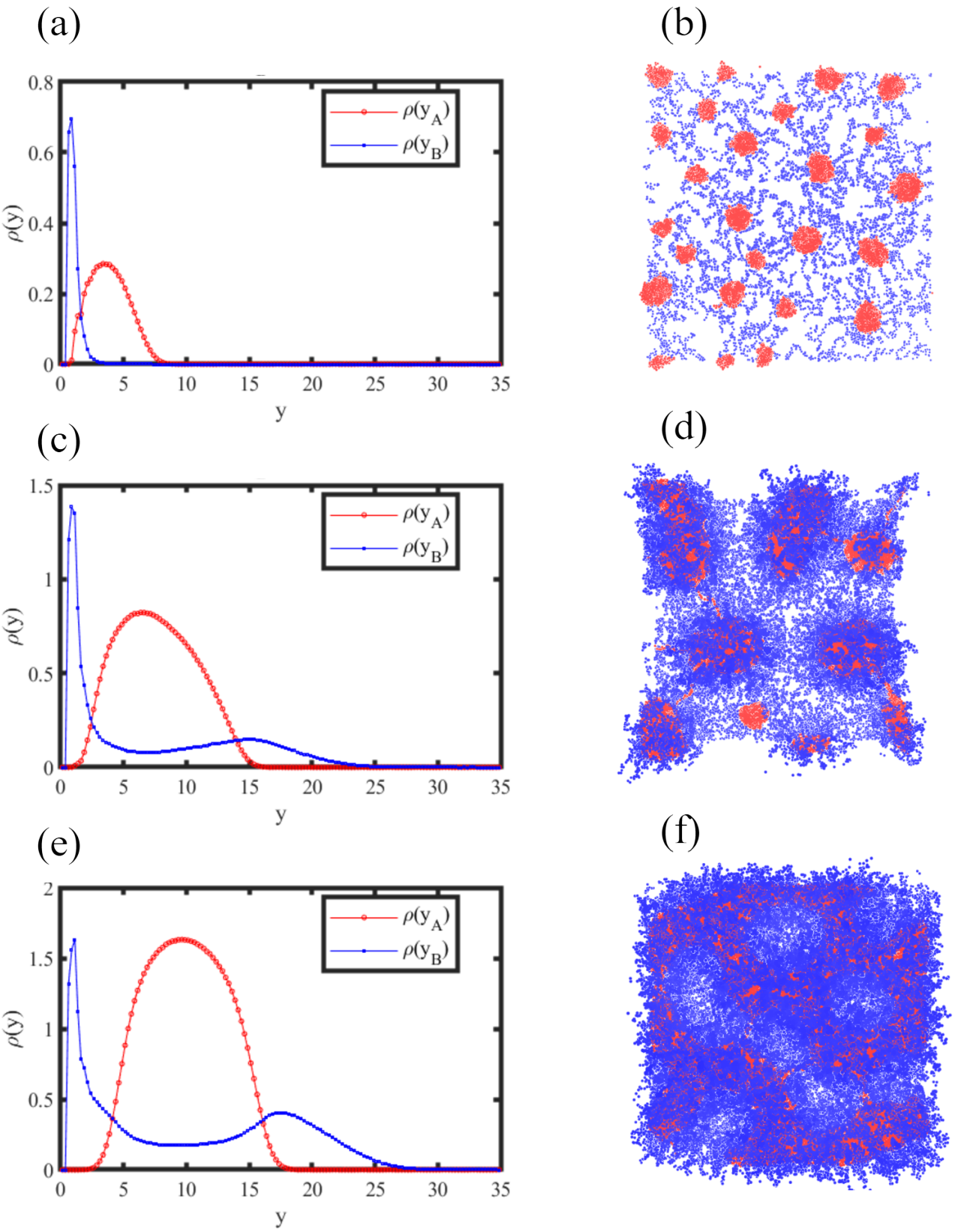

Figure S5: Density profiles (left) and top-view snapshots (right) corresponding to the curves shown in figure 5 in the main text. Three relevant values of the nominal B coverage are shown: $\sigma_B^* = 0.6$ for (a) and (c); $\sigma_B^* = 3.6$ for (a) and (c); and $\sigma_B^* = 7.9$ for (a) and (c);